ISSN: 2472-3703 DOI: 10.6911/WSRJ.202509_11(9).0002

Modal Analysis and Optimization of Electric Vehicle Chassis Structure

Kaiyan Wang[1, a], Pei Wang[2, b], Ye Lin[3, c], Xin Wang[4, d]

[1]School of Automobile and Transportation Shenyang Ligong University, Shenyang, China

[2]R&D Institute Chery Automobile Co., Ltd., Wuhu, China

[3]Vehicle Development Department R&D Center, FAW GROUP Changchun, China

[4]Changchun Fawsn Anchuang Automotive Parts Co., Ltd Changchun, China

[a]wangky@sylu.edu.cn, [b]2728679258@qq.com, [c]linye2@faw.com.cn, [d]xin.wang@fawsnac.com

Abstract

The interior noise of electric vehicles (EVs) at low velocities is predominantly attributed to structural vibrations. This study proposes a systematic optimization of the EV chassis structure through modal analysis, integrated with spectral characteristics of interior noise. Initially, finite element models of critical chassis components were developed and validated via experimental modal testing. Subsequent the modal frequency and vibration mode of each component were obtained by finite element analysis. By correlating the frequency spectrum of interior noise with the chassis modal frequencies, the rear subframe and strengthening plates were identified as priority optimization targets. Targeted structural reinforcements were implemented to elevate the natural frequencies of these components, thereby achieving effective frequency avoidance and mitigating structural vibrations. The proposed methodology demonstrates a data-driven approach to enhance NVH (Noise, Vibration, and Harshness) performance of the vehicle.

Keywords

Electric Vehicle, Chassis structure, Modal Analysis, Optimization.

1. INTRODUCTION

Compared to internal combustion engine vehicles (ICEVs), Evs exhibit reduced interior noise due to the absence of engine-related masking effects. However, road noise, wind noise, and electric drivetrain system noise become more pronounced in EVs [1-2]. At low to medium speeds, road noise emerges as the primary contributor to EVs NVH performance[3]. During such operating conditions, road excitations are transmitted through the chassis structure into the cabin, where they interact with chassis components via vibration coupling, ultimately inducing structural vibrations and interior noise issues [4].

Research demonstrates that the EV chassis serves as the primary structural pathway for mechanical force transmission, with the coupling between its modal characteristics and noise spectrum directly influencing vibration transmission efficiency. Zhu et al. identified that modal coupling of the rigid-body mode of the electric drive assembly and the acoustic cavity mode can induce low-frequency booming noise [5]. However, existing studies predominantly focus on optimizing individual powertrain components (e.g., motors, gear reducers), while the modal of the integrated chassis structure and its correlation with noise generation remain insufficiently investigated [6-7]. Furthermore, conventional chassis design methodologies developed for

ISSN: 2472-3703 DOI: 10.6911/WSRJ.202509_11(9).0002

ICEVs are ill-suited to address EV-specific requirements. Notably, novel design constraints such as battery pack integration and electric drivetrain mounting impose heightened demands on chassis stiffness distribution to mitigate NVH issues [8].

This study addresses structural noise issues in EVs under low-speed operating conditions. The finite element model of critical chassis components—including front/rear subframes and control arms—is initially developed and validated against modal testing data to ensure model fidelity. Subsequent comparative analysis with vehicle test results identified components susceptible to modal coupling phenomena. To mitigate these issues, a targeted structural reinforcement strategy is proposed, where localized stiffening measures are implemented to elevate the natural frequencies of the chassis components. This approach achieves frequency avoidance relative to excitation frequencies, thereby suppressing structural noise propagation pathways within the EV chassis system.

2. PRINCIPLES OF MODAL ANALYSIS

Modal characteristics represent the inherent vibration properties of a structural system, which remain invariant once the system configuration is established, independent of external excitation conditions. Each modal order is characterized by specific parameters, including natural frequency, damping ratio, and vibration mode shape. Through finite element analysis of critical vehicular components, their natural frequencies can be systematically identified and quantified[9].

Modal analysis involves discretizing the physical structure into an equivalent multi-degree-of-freedom vibration system. When structural damping is considered, the governing equation of motion for free vibration can be formulated as:

$$[M]\{\ddot{x}\} + [C]\{\dot{x}\} + [K]\{x\} = \{F(t)\} \tag{1}$$

Where: $[M]$ is mass matrix, $[C]$ is damping matrix, $[K]$ is stiffness matrix, $\{x\}$ is displacement vector, $\{F(t)\}$ is excitation force

For the chassis system in an unconstrained free state, damping effects and external excitations are negligible in modal analysis, as the structural response is dominated by inherent dynamic properties. Under this condition, the system is modeled as a multi-degree-of-freedom undamped vibration system. Consequently, the equation of motion simplifies to:

$$[M]\{\ddot{x}\} + [K]\{x\} = 0 \tag{2}$$

Under the assumption of simple harmonic motion, the displacement response of the system can be represented analytically as:

$$X = A\sin(\omega t + \Phi) \tag{3}$$

Where：A is the amplitude vector, ω is the angular frequency, ϕ is the phase angle.

Substituting Eq. (3) into Eq. (2) yields the following equation:

$$([K] - \omega^2[M])A = 0 \tag{4}$$

ISSN: 2472-3703 DOI: 10.6911/WSRJ.202509_11(9).0002

When the coefficient determinant of Eq. (4) is 0, there is a non-zero solution, that is :

$$K - \omega^2 = 0 \tag{5}$$

Since both the stiffness matrix and mass matrix are n×n matrices, the governing equation yields n distinct solutions. These solutions correspond to the n natural frequencies of the structural system, which are determined through eigenvalue analysis. The eigenvectors associated with each natural frequency, as derived from Eq. (5), represent the system's natural vibration modes.

3. FINITE ELEMENT MODELING OF CHASSIS COMPONENTS

Constrained modal analysis enables the characterization of chassis components' modal under operational installation conditions, thereby providing a high-fidelity representation of their dynamic characteristics during operational conditions. Constrained modal analysis requires the incorporation of boundary conditions into the simulation model, which should accurately replicate the actual mounting configurations of the components as installed in the vehicle system.

3.1. Finite Element Model of Subframe

The front subframe, a thin-walled structural component fabricated from sheet metal, is discretized using a 5 mm × 5 mm shell element mesh. A hybrid meshing strategy combining triangular and quadrilateral elements is used to ensure geometric fidelity while maintaining computational efficiency. The primary material exhibits an elastic modulus of 205 GPa, poisson's ratio of 0.3, and density of 7850 kg/m^3. Bolt connections are modeled using double-layer rigid beam elements (RBE2 formulation) to replicate interfacial stiffness characteristics. Fixed boundary conditions are applied at subframe-body attachment points, with lumped masses distributed at these locations to account for simplified representations of powertrain components. The mesh discretization, material properties, and joint configurations of the rear subframe mirror those of the front subframe. A rotational degree of freedom is incorporated between the rear subframe and control arm assembly, simulating the kinematic coupling through a revolute joint. The finite element models of front and rear subframe are as shown in Fig. 1.

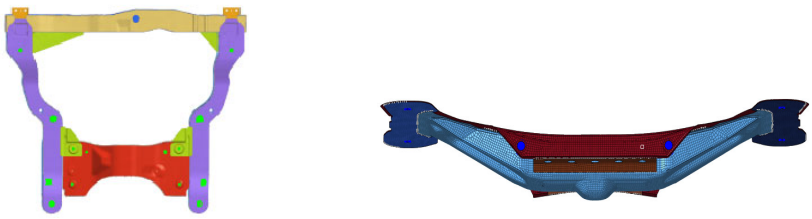

(a) (b)

Figure 1. Front subframe model (a:front subframe, b: rear subframe)

3.2. Finite Element Model of Strengthening Plate

A total of three strengthening plates are connected to both the subframe and vehicle body via bolted joints. These plates are discretized using 5 mm × 5 mm shell elements, with material properties identical to those of the subframe. Fixed boundary conditions are applied at the plate-subframe interface to replicate rigid mounting characteristics. The finite element models of strengthening plates are as shown in Fig. 2.

ISSN: 2472-3703 DOI: 10.6911/WSRJ.202509_11(9).0002

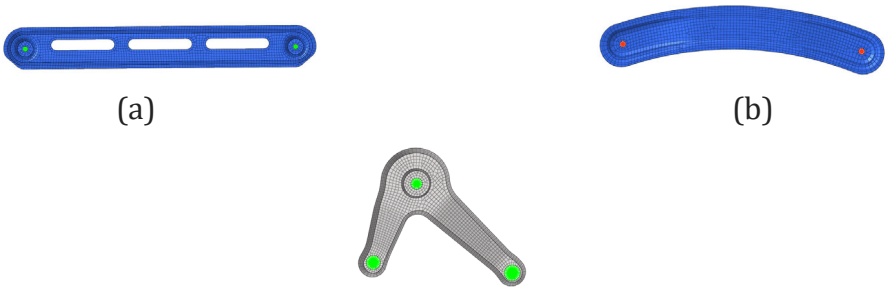

(a) (b)

(c)

Figure 2. Strengthening plates model (a: strengthening plate A, b: strengthening plate B, c: strengthening plate C)

3.3. Finite Element Model of Lower Swing Arm

The lower swing arm is discretized using a 5 mm × 5 mm solid element mesh. The component is fabricated from SAPH440 automotive structural steel, exhibiting an elastic modulus of 207 GPa, poisson's ratio of 0.3, and density of 7800 kg/m^3. Bolt connections are modeled using RBE2, with a revolute joint implemented at the subframe interface to permit rotational degrees of freedom. The finite element model of lower swing arm is as shown in Fig. 3.

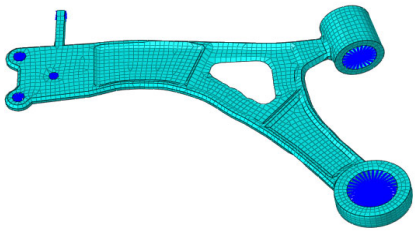

Figure 3. Lower swing arm model

3.4. Finite Element Model of Stabilizer Bar

The front and rear stabilizer bars are discretized using 5 mm × 5 mm quadrilateral shell elements. The isotropic material model is defined by an elastic modulus of 207 GPa, poisson's ratio of 0.3, and density of 7800 kg/m^3. Spherical joint elements are employed to simulate the rotational degrees of freedom at bar-linkage interfaces. The finite element model of stabilizer bars are as shown in Fig. 4 and Fig. 5.

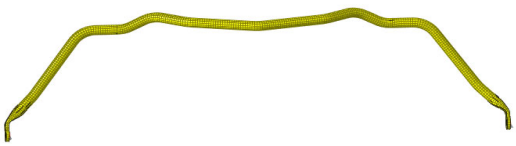

Figure 4. Front stabilizer bar model

Figure 5. Rear stabilizer bar model

ISSN: 2472-3703 DOI: 10.6911/WSRJ.202509_11(9).0002

3.5. Finite Element Model of Control Arm

The front toe control arm, along with the upper and lower control arms, are discretized using a 5 mm × 5 mm shell element mesh. The components are fabricated from SAPH590 automotive structural steel, characterized by an elastic modulus of 206 GPa, Poisson's ratio of 0.3, and density of 7830 kg/m^3. Bolt connections are modeled using RBE2 to replicate interfacial stiffness characteristics. A rotational degree of freedom is set for each bolt connection of the control arms. The finite element model of control arms are as shown in Fig. 6.

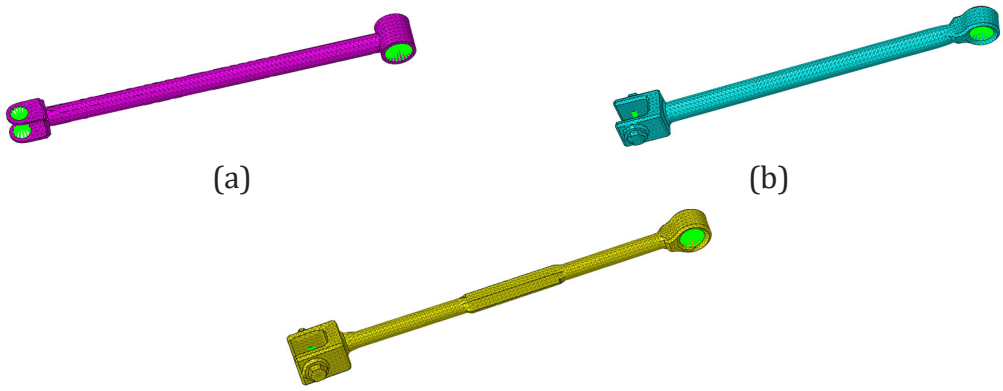

Figure 6. Control arm model (a: front toe control arm, b: upper control arms c: lower control arms)

4. MODAL TEST AND MODEL VALIDATION

Following the establishment of the finite element model, modal analysis is conducted to extract the modal frequencies and corresponding vibration modes of the chassis components. The model is subsequently validated through modal test, which is performed in-situ under full vehicle installation conditions. Components are excited using an impact hammer methodology implemented in LMS Test Lab test system, with test parameters configured at a sampling frequency of 2048 Hz and frequency resolution of 1 Hz. The modal test is as shown in Fig. 7.

Figure 7. Modal test of chassis components

Comparative analysis of modal test and simulation results, as presented in Table 1, reveals that the maximum discrepancy in first-order bending and torsional mode frequencies for all components are constrained to within 10%. This error margin satisfies the accuracy requirements for engineering applications, confirming the validity of the model.

ISSN: 2472-3703 DOI: 10.6911/WSRJ.202509_11(9).0002

Table 1. Modal of Chassis Components

Component	Test Frequency (Hz)	Simulation Frequency (Hz)	Relative Error (%)	Mode
Front subframe	89	88	1.10	1st bending
	228	232	1.70	1st torsion
Rear subframe	86	83	3.50	1st bending
	127	123	3.10	1st torsion
Strengthening plate A	152	143	5.90	1st bending
	331	339	2.40	1st torsion
Strengthening plate B	147	140	4.80	1st bending
	264	286	8.30	1st torsion
Strengthening plate C	134	146	8.90	1st bending
	171	164	4.10	1st torsion
Lower swing arm	148	157	6.10	1st bending
	255	245	3.90	1st torsion
Front Stabilizer bar	76	73	3.90	1st bending
	146	144	1.40	1st torsion
Rear Stabilizer bars	78	75	3.80	1st bending
	184	186	1.10	1st torsion
Front toe control arm	62	68	9.60	1st bending
	324	336	3.70	1st torsion
Upper control arm	137	143	4.30	1st bending
	553	547	1.1	1st torsion
Lower control arm	229	216	5.70	1st bending
	567	549	3.20	1st torsion

5. CHASSIS STRUCTURE OPTIMIZATION

5.1. Identification of Critical Chassis Components

Interior noise tests are conducted during constant-speed vehicle operation at 40 km/h, revealing prominent tonal peaks at 80 Hz and 160 Hz. Transfer Path Analysis (TPA) is subsequently performed to identify dominant noise transmission pathways contributing to these critical frequencies[10]. By decomposing frequency-domain contributions from individual chassis components, prioritized optimization candidates are determined based on path dominance criteria. Test results of each structural and vibrational pathway's contribution to cabin noise is presented in Fig.8

(a) (b)

Figure 8. Cabin noise contribution of chassis components transfer paths (a:80Hz, b: 160Hz)

ISSN: 2472-3703 DOI: 10.6911/WSRJ.202509_11(9).0002

Transfer Path Analysis of the 80 Hz noise, as shown in Fig. 8(a), identify significant contributions from the right-rear and left-rear mounting interfaces of the rear subframe. Modal analysis of the chassis components reveal a structural resonance mode of the rear subframe near 80 Hz. This finding, coupled with experimental frequency response data, establishes a direct causal relationship between the subframe and the interior noise at this frequency. The resultant frequency coupling confirms that the rear subframe are the dominant contributor to the interior noise issue at 80 Hz.

Transfer Path Analysis of the 160 Hz noise, as shown in Fig. 8(b), identify significant contributions from the right-rear and left-rear mounting interfaces of the front subframe. Modal analysis identify resonance modes near 160 Hz for both structural strengthening plates (plate A and plate C). Notably, plate C is mounted at the rear attachment points of the front subframe. This frequency coupling phenomenon confirms that resonant excitations of plate A and plate C are the primary contributors to the interior noise issue at 160 Hz.

5.2. Structure Optimization

1. Rear subframe

To enhance structural integrity at the identified weak regions near the four body-subframe mounting interfaces, a 2 mm-thick high-strength steel strengthening plate is implemented, as schematically illustrated in Fig. 9.

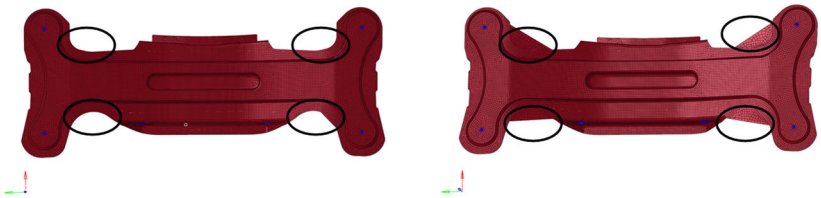

(a) (b)

Figure 9. Structure improvement of rear subframe (a: before improvement, b: after improvement)

The modal results of the improved subframe are compared with those before the improvement, as shown in Table 2. After improvement, the first-order bending frequency is increased by 19 Hz to 102 Hz, and the first-order torsion frequency is increased by 16 Hz to 139 Hz. The modal frequency of the improved rear subframe avoids the frequency range of 80 Hz.

Table 2. Improvement Results of Rear Subframe

Frequency (Hz)		Variance ratio (%)	Mode
Before improvement	After improvement		
83	102	22.8	1st bending
123	139	13	1st torsion

2. Strengthening plate A

To address localized stiffness deficiencies in strengthening plate A, two trapezoidal stiffening ribs with dimensions of 5 mm (width) × 10 mm (height) are precision-pressed into the critical section, as schematically detailed in Fig. 10.

ISSN: 2472-3703 DOI: 10.6911/WSRJ.202509_11(9).0002

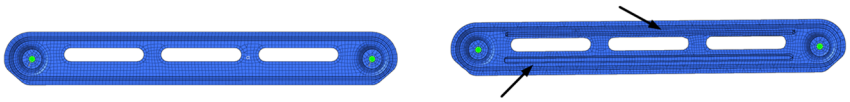

Figure 10. Structure improvement of strengthening plate A (a: before improvement, b: after improvement)

The modal results of the improved strengthening plate a are compared with those before the improvement, as shown in Table 3. After improvement, the first-order bending frequency is increased by 69 Hz to 212 Hz, and the first-order torsion frequency is increased by 320 Hz to 659 Hz. The modal frequency of the improved strengthening plate a avoids the frequency range of 160 Hz.

Table 3. Improvement Results Of Strengthening plate A

Frequency (Hz)		Variance ratio (%)	Mode
Before improvement	After improvement		
143	212	48.2	1st bending
339	659	94.3	1st torsion

3. Strengthening plate C

To address localized stiffness deficiencies in strengthening plate C, a 10 mm-wide steel flange with 2 mm thickness is implemented at the critical section, as shown in Fig.11.

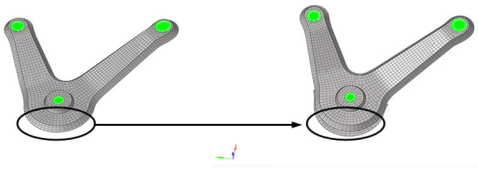

(a) (b)

Figure 11. Structure improvement of strengthening plate C (a: before improvement, b: after improvement)

The modal results of the improved strengthening plate care compared with those before the improvement, as shown in Table 4. After improvement, the first-order bending frequency is increased by 35 Hz to 169 Hz, and the first-order torsion frequency is increased by 15 Hz to 186 Hz. The improved c-mode frequencies of the strengthening plate avoid the frequency range of 160 Hz.

Table 4. Improvement Results of Strengthening plate C

Frequency (Hz)		Variance ratio (%)	Mode
Before improvement	After improvement		
134	169	26.1%	1st bending
171	186	8.7%	1st torsion

6. CONCLUSION

1) High-fidelity finite element models of critical chassis components—including front/rear subframes, stabilizer bar, lower swing arm, and structural strengthening plate—were

ISSN: 2472-3703 DOI: 10.6911/WSRJ.202509_11(9).0002

developed. Modal validation against experimental data revealed frequency discrepancies below 10% across all critical modes, confirming the models' exceptional predictive accuracy.

2) Employing TPA methodology, dominant noise propagation pathways at 80 Hz and 160 Hz were systematically identified. Correlation of these findings with modal analysis revealed a critical vibration coupling phenomenon between the rear subframe, strengthening plate A, and C.

3) Targeted structural optimizations were implemented through localized stiffening of the rear subframe and reinforcement components. Post-optimization modal analysis revealed significant frequency shifts: the optimized subframe exhibited a first-order bending frequency increase of 19 Hz and a first-order torsional frequency increase of 16 Hz. Strengthening plate A demonstrated a pronounced first-order bending frequency enhancement of 69 Hz and a torsional frequency increase of 320 Hz. Similarly, strengthening plate C achieved a first-order bending frequency elevation of 35 Hz and a torsional frequency increase of 15 Hz. These strategic modifications effectively shifted resonant frequencies away from problematic operational bands, thereby mitigating vibrational coupling issues across the chassis system.

ACKNOWLEDGMENTS

This work is financially supported by basic scientific research projects of the Liaoning Provincial Department of Education (LJKMZ20220603).

REFERENCES

[1] Kang Q, Gu P , and Li J, et al. A Research on the Evaluation Method of High-frequency Whining Noise in Electric Drivetrain[J]. Automotive Engineering, 2019,41(06):682-687.

[2] Hua X, Thomas A, Shultis K. Recent progress in battery electric vehicle noise, vibration, and harshness[J]. Science Progress, 2021, 104(1): 00368504211005224.

[3] Yu W. Analysis and Optimization of Low-Speed Road Noise in Electric Vehicles[J]. Wireless Communications and Mobile Computing, 2021, 2021(1): 5537704.

[4] Yu Z, Cheng D, Huang X. Low-frequency road noise of electric vehicles based on measured road surface morphology[J]. World Electric Vehicle Journal, 2019, 10(2): 33.

[5] Zhu J, Zheng T, and Lv Y, et al. Description and Optimization for Common Noise and Vibration Problems of Electric Vehicle[J]. Automobile Applied Technology, 2020, (01): 214-220.

[6] Shen L, Zhang J, and Zhao M, et al. Booming Noise Analysis and Control Strategy Optimization of an Electric Vehicle in Creep Condition[J]. Noise and Vibration Control, 2024,44(06):219-223+297.

[7] Yu H, Zhang T, Ma Z, et al. Torsional vibration analysis of planetary hybrid electric vehicle driveline[J]. Transactions of the Chinese Society of Agricultural Engineering, 2013, 29(15): 57-64.

[8] Lu Y, Mao H, Zhou M. Topology optimization of electric vehicle chassis structure with distributed load-bearing batteries[J]. Structural and Multidisciplinary Optimization, 2023, 66(6): 134.

[9] Barbosa L M Q, Fernandes G H N, de Queiroz Murad M.. Finite element analysis and optimization of a Formula SAE car chassis[J]. Caderno Pedagógico, 2024, 21(1): 2053-2071.

[10] Nataraja Moorthy S, Rao M V, Raghavendran P, et al.. NVH Optimization of Mounts for Reduction of Structure Borne Motor and Road Noise in Electric Vehicle[J]. SAE Technical Paper, 2025: 28-0072.